Experimental Stark widths of Kr III

I. Ahmad,* S. Büscher, Th. Wrubel, and H.-J. Kunze
Institute for Experimental Physics V, Ruhr-University-Bochum, 44780 Bochum, Germany
(Received 12 June 1998)

We present Stark width measurements of three strong Kr III lines of the $(5s\,^5S^o-5p\,^5P)$ quintet. The measurements are performed in a plasma produced in the gas-liner pinch, which is equipped with a Thomson scattering system as an independent plasma diagnostic. The investigation shows that the lines are emitted spatially homogeneous and optically thin, thus an experimental scaling law of the Stark width with electron density can be presented. Another plasma regime with a density variation along the *z*-axis can be cultivated by an unusual strong seeding of the hydrogen plasma with krypton ions. This large amount of test gas injection produces inhomogeneous spectra along the *z* axis. The nonuniformity of the emission of the spectral lines is attributed to an inhomogeneity of the plasma column resulting from instabilities generated in the compression phase of the plasma. [S1063-651X(98)06811-1]

PACS number(s): 52.70.Kz, 32.70.Jz

INTRODUCTION

Since the 1960s, due to the explosive growth of new and promising technologies, krypton gas has come into ever increasing practical use especially for the manufacturing of particular types of light sources and lasers [1,2]. Recently krypton has gained some attention to generate short-wavelength lasers as well [3]. One of the outstanding challenges on the way to a fusion reactor is the problem of energy exhaust [4]. Towards the solution of this problem the concept of a cold radiative plasma boundary has been reviewed quite recently [5]. In a fusion machine like ITER (International Thermonuclear Experimental Reactor) krypton may play a practical role for distributing a substantial fraction of the power on the various parts of the wall of the reactor.

In order to realize such applications details of atomic data have to be known. In the following we present a study of the Stark width of three strong components of Kr III originating from the same multiplet. They are in the uv spectral range: (i) $\lambda=335.193$ nm, $5s\,^5S^o-5p\,^5P$, $J=2-1$, (ii) $\lambda=332.575$ nm ..., (iii) $\lambda=334.569$ nm ..., $J=2-3$ and provide data for comparison with calculations. At present, only calculations by Hey [6] are available, which were obtained using a code according to Refs. [7,8]. One deficiency in this regard is the extremely poor knowledge of the energy levels especially of levels with high principal quantum numbers. Although some data in the vuv (vacuum ultraviolet) and near uv region of the spectrum are available, they are inadequate for the complete knowledge of the energy levels [9–15]. Therefore, theoretical Stark width calculations for these transitions are not yet available.

Measurements of the Stark width and its scaling with density in multiply ionized atoms have attracted considerable attention in recent years, especially after discrepancies between theory and experiment have been found [16–18]. The gas-liner pinch has been employed quite extensively since its inception for such investigations [19–23]. One goal of a series of experiments at the gas-liner pinch is to test the theories of Stark broadening so that these can be applied to the diagnostic of high-density plasmas and to opacity calculations. Many of the former measurements of ions in lower ionization stages [24–29] fit within their error bars to theoretical profiles predicted by various authors [30,31,7,8], but discrepancies between theory and experiment have been seen as well. Moreover, different theoretical assumptions predict line profiles whose Stark widths differ significantly. As an example, even within the framework of the semiclassical approach of electron broadened isolated lines, the estimates of the contribution of strong collisions differ [8]. A recent improvement of the semiclassical estimate of the strong collision term and the inclusion of higher order terms [32] led to an overall good agreement between semiclassical calculations and the experiment [33] even for ''high'' Z ions ($Z\leqslant 8$). For the interpretation of the broadening of the resonance transition of B III measured at the gas-liner pinch [34], it has been suggested [16] that some kind of hydrodynamic turbulence might be generated in the pinch plasma resulting in increased Doppler broadening, which is erroneously attributed to Stark broadening. The corresponding quantum mechanical result is lower than the experimental width by a factor of 2, but the experimental width is again consistent with semiclassical calculations [7,8].

I. EXPERIMENTAL SETUP AND DIAGNOSTICS

The gas-liner pinch device shown in Fig. 1 has been described from its first design [35–38] to the present setup [18,29,33]. Briefly, it resembles a large aspect ratio *z* pinch consisting of two parallel electrodes of diameter 18 cm and 5 cm apart. Special features of the device are two independent fast electromagnetic valve systems providing concentric gas streams, one as a hollow cylindrical shell near the wall called the driver gas. The other valve injects the so-called test gas along the axis of the discharge through a nozzle in the center of the upper electrode. High reproducibility of the device is ensured by a pre-ionization system. The amount of test gas can be varied from a few tenths of a percent to several per-

*Permanent address: Department of Physics, Quaid-i-Azam University, Islamabad, Pakistan.

 © 1998 The American Physical Society

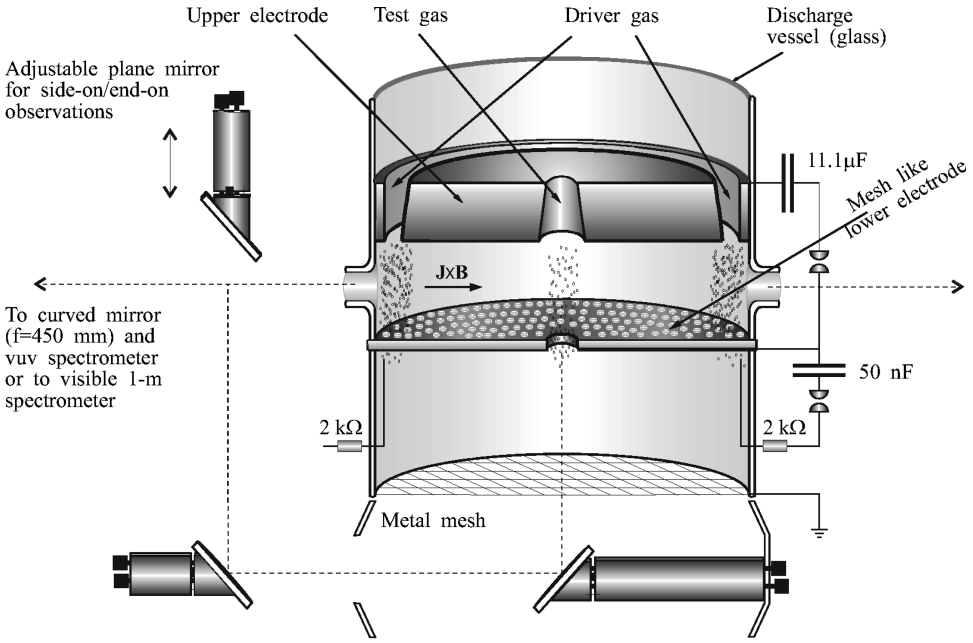

FIG. 1. Schematic of the gas-liner pinch.

cents of the driver gas. The injection time is adjusted in such a manner that a proper amount of impurity ions persists in a homogeneous central part of the plasma and a cold boundary layer of the test gas ions is practically absent [39]. The device is energized by a 11.1-μF main capacitor bank charged up to 20–45 kV, providing 2.2–11.2 kJ discharge energy.

A $\frac{1}{4}$-m monochromator (ISA, Jobin Yvon) is employed to monitor the time behavior of the plasma continuum radiation at a wavelength of 520 nm. The plasma parameters are determined simultaneously with the spectroscopic observation by collective Thomson scattering. The diagnostic system consists of a ruby laser (Korad K1-Q, 50 MW) having a pulse duration of about 30 ns. The laser beam is focused into the geometrical center of the discharge vessel. The scattered light from the center is collected at a scattering angle of 90° and is focused onto the entrance slit of a 1-m spectrograph (Spex model 1704) mounted with a 1200-lines/mm grating blazed at 1000 nm. In the exit plane of the spectrograph an optical multichannel analyzer (OMA II, EG&G model 1456-990G) is mounted, giving a linear reciprocal dispersion of 6.3 pm/pixel in second order. For the spectroscopic measurements we employed an intensified charge coupled device (ICCD 578×384, Princeton Instruments) to detect spectral lines spatially resolved. The ICCD system is installed at another 1-m spectrograph (Spex M1000) containing a 1200-lines/mm grating blazed at 750 nm. The linear reciprocal dispersion of the spectroscopic system is 18.2, 8.7, and 5.2 pm/pixel in first, second, and third order, respectively. The dispersion has been determined by employing cold spectral lamps.

In an effort to answer some of the questions mentioned in the Introduction, we performed a detailed analysis of the plasma dynamics via radially resolved Thomson scattering measurements [40]. We showed that the plasma column formed is homogeneous and free of turbulence when a small amount of test gas is injected. Moreover, the density is constant over 1.0 cm around the z axis and the spectral lines are not affected by self-absorption due to the absence of a cold boundary layer. For extreme discharge conditions (i.e., the case of a large amount of test gas injection) Thomson scattering gives a hint to incipient instabilities, but it is revealed that the effects of instabilities and turbulence vanish at later times of the discharge and the plasma column seems to relax macroscopically. For the present Stark profile measurements we used a very small amount of test gas ($<1\%$ of the driver gas) and, in addition, the lines appeared at late times after maximum pinch compression. These are satisfactory experimental conditions; for that reason we are certain that for the Stark width measurements presented here there are no additional Doppler effect contributions caused by macroscopic motion and turbulence that could affect the line profiles.

It is important to study the inhomogeneity arising with large amounts of test gas. Therefore we created in a second step such an inhomogeneous condition. The electron density is axially resolved and determined by the Stark width of the Kr III quintet lines.

II. EXPERIMENTAL RESULTS AND DISCUSSION

A. Density scaling of the Stark width

We measured three components of the quintet ($5s\,^5S^o - 5p\,^5P$) of Kr III ions at wavelengths of $\lambda = 335.193$ nm ($J=2-1$), $\lambda = 332.575$ nm ($J=2-2$), and $\lambda = 324.569$ nm ($J=2-3$). It was possible to measure the lines in first, second, and third order, but due to the high resolution and the ICCD chip size all three components could not be measured together; in first and second order each two neighbored components appeared. We measured the spectral lines at wavelengths $\lambda = 335.193$ nm and $\lambda = 332.575$ nm together in first and second order. The spectral line at wavelength $\lambda = 332.575$ nm was also measured along with the line at $\lambda = 324.569$ nm in first order. Second order measurements of the line at wavelength $\lambda = 324.569$ nm and third order measurements of the line at wavelength $\lambda = 332.575$ nm have also been made.

We performed measurements with a low amount of test gas injection (up to 1%) to check if the intensity ratio and

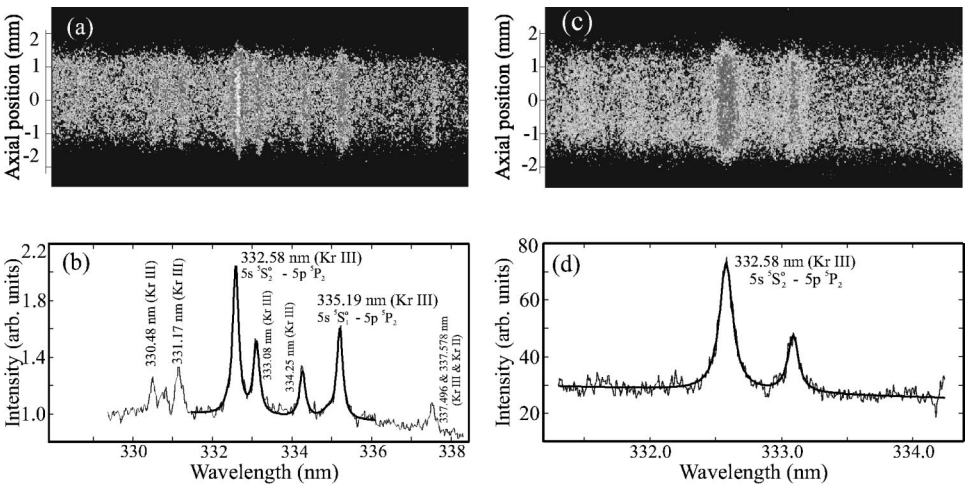

FIG. 2. Examples of measured spectra of $5s\,^5S_2^o - 5p\,^5P_2$ Kr III in first (a), (b) and third (c), (d) order: The $(J=2-1)$ component measured in first order is also shown. The spectra in (b), (d) are the mean of the corresponding ICCD spectra over the height together with their best fits. Zero position in the ICCD spectra corresponds to the midplane of the discharge volume.

width ratio of the lines under investigation remain the same or if they vary with the amount of injected test gas. In this set of measurements we ensured that the emission was spatially homogeneously distributed. We found that the intensity ratio and the width ratio of the lines remain invariant with the amount of injection and the ratios are within the error bars equal to those predicted by the LS coupling scheme as will be discussed later.

One of the ICCD spectra recorded in first order is shown in Fig. 2(a). In the ICCD spectra shown in Fig. 2 the top and the bottom portions are black due to the slit height, which was nearly 4 mm. The central position was determined by placing a lamp at the geometrical center of the discharge. Figure 2(b) gives the corresponding line profile obtained by taking the mean of the vertical (i.e., axial) channels, where the gray line gives the experimental data points and the black solid line is the best theoretical fit to the data points. The experimental lines were fitted independently with a Voigt profile that consists of a Lorentzian profile accounting for Stark broadening, which was numerically convoluted with the apparatus profile and the Doppler profile. The apparatus profile has a width [full width at half maximum (FWHM)] of about 3.1 pixel. To estimate the contribution of the Doppler part we have determined the ion temperature for the whole set of measurements by Thomson scattering. For the krypton ions the contribution of the Doppler part is practically negligible in the range of our plasma temperature of 3 eV $\leqslant k_B T_e \leqslant 6$ eV. From the figures it is evident that the fit of the theoretical profile to the experimental data is very good. We fitted additional Voigt profiles to lines that are near the wings of the lines of interest. The first and second order measurements were used to determine the intensity ratio of the lines. The experimental intensity ratios are $(0.94 \pm 13\%):1.7:(2.64 \pm 8\%)$ for Kr III $J=2-1$, $J=2-2$, $J=2-3$, respectively.

To determine the theoretical intensity ratio we estimated the electron collision rate and the radiative decay rate [41]. For the plasma parameters in our range the electron collision rate is 500 times higher than the radiative decay rate. Therefore, the population densities of the two levels are according to the Boltzmann distribution, and assuming LS coupling the intensity ratio can be written as [41]

$$\frac{I_1}{I_2} = \frac{\lambda_2}{\lambda_2}\frac{g_1 f_1}{g_2 f_2}\exp\left(\frac{E_2 - E_1}{k_B T_e}\right), \tag{2.1}$$

where λ, g, and f are the wavelength, statistical weights, and oscillator strength of the levels, respectively. Unfortunately, for the lines under investigation f values are not available in the literature; however, one may assume that they are equal since for most of the cases f does not change much within the same multiplet [42]. For such transitions between levels of high principal quantum number predictions of LS coupling should be valid because the valence electron is far away from the parent electrons and the core. Under this assumption the theoretical value of the intensity ratio is 1:1.7:2.5. If we compare the theoretical value of the intensity ratios with the experimental value we see that the agreement is very good. The widths of the three components are equal within their error bars, the ratio of the width of the stronger component to that of the weaker component is $0.97 \pm 14\%$. All together, the intensity and width ratios confirm that the lines are emitted optically thin. The standard deviation of the spectral shift is of the three components is less than one pixel, which reveals that the plasma is macroscopically stationary for the whole duration of the measurements. In addition, the spectral lines have been found at the tabulated wavelength positions of Ref. [43].

For the absolute width measurements higher order measurements are preferable for the following reasons: The reflectivity of the grating is higher due to the blaze angle. As mentioned, the apparatus profile is about 3.1 pixel, it contributes up to 44%, 21%, and 16% of the total width in first, second, and third order, respectively. For the higher order measurements we have introduced an optical filter UG5 [44] into the optical path, which has about 99% transmission in the wavelength range of $\lambda = 300-500$ nm. In the wavelength range $\lambda = 600-650$ nm and $\lambda = 900-1000$ nm its transmission is (0.5–5)% and 60%, respectively. Therefore, for the second order measurements the filter will completely cut any first order contribution arising from lines at the longer wavelengths. In third order measurements the filter will also significantly reduce the effect of first order contributions at the longer wavelengths. One of the ICCD spectra recorded in third order is depicted in Fig. 2(c). The corresponding line profile averaged over the vertical channels is

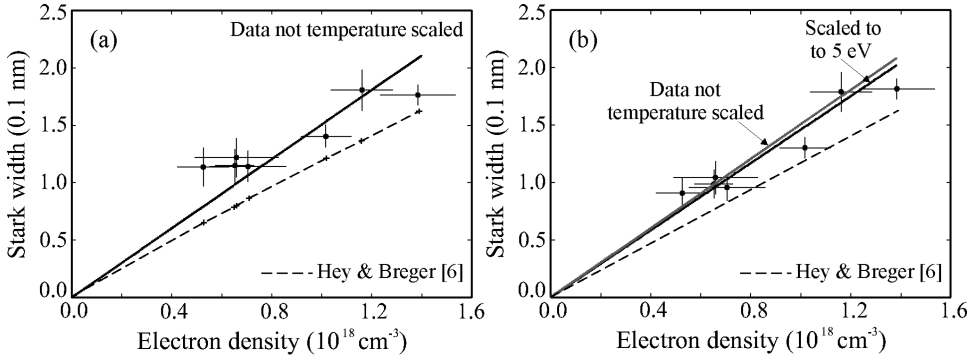

FIG. 3. Stark width vs electron density together with corresponding theoretical values of [6]. (a) shows the data without any temperature scaling with their best linear fit. (b) shows the width scaled to a temperature 5 eV using a $1/\sqrt{k_B T_e}$ dependence together with their best fit. For comparison the fit of the unscaled data is also given.

shown in Fig. 2(d). We note that for the higher order measurements an overall fitting of the theoretical profile to the experimental profile is better compared to the first order measurements because the assumption of a linear continuum contribution is fulfilled better.

In Fig. 3(a) the width versus density graph for all the components measured in higher orders is given where each data point represents the mean of about 10 shots. In order to investigate the pure density dependence of the experimental Stark width one has to account for the temperature variation. Theoretically the Stark width is proportional to the product of $1/\sqrt{k_B T_e}$ and the Gaunt factors summed up over all the perturbing levels. If the energy of the perturbing electron is less than twice the energy difference between the perturbing levels the Gaunt factors have nearly temperature independent [45]. This holds if the electron temperature is very low, thus giving a $1/\sqrt{k_B T_e}$ dependence of the Stark width. In the opposite regime, if the energy of the perturbing electron is comparable to or even larger than the energy difference of the perturbing levels, Gaunt factors are temperature dependent. At high temperatures the temperature dependence of the Gaunt factors will counteract that of the factor $1/\sqrt{k_B T_e}$, thus giving a temperature independent Stark width. For our case we are in the intermediate regime due to the moderately large principal quantum number and the low temperatures where the exact dependence on the temperature is not known. Therefore, in Fig. 3(b) we have shown the experimental Stark widths for the two extreme cases. The data points are scaled to a temperature of 5 eV using the $1/\sqrt{k_B T_e}$ dependence, and they are shown together with their best fit. The fit of the unscaled data points [of Fig. 3(a)] is shown as well. There is no significant change between these fits, which is obviously due to the small temperature range covered by our experiment. Therefore, we present the following electron density scaling of the Stark width:

$$w_s(\mathrm{nm}) = 0.146 \times 10^{-18} n_e(\mathrm{cm}^{-3}). \qquad (2.2)$$

The uncertainty of the linear fit to the experimental data is about 15%, which includes also the error arising from density diagnostics. This scaling is recommended for an electron temperature of about 5 eV. The complete experimental data set of the Stark widths (FWHM) for the measurements is given in Table I.

Figure 3 also shows the results of a calculation for the strongest line ($5s\,^5S_2^o - 5p\,^5P_3$) of the Kr III multiplet [6], with strong collision contributions included for both the upper and the lower states of the line. This calculation treats only the line broadening by electron perturbers, within the classical path and the impact approximations. In spite of the rather poorly known term scheme for this ion, a surprisingly high degree of completeness of the perturbing levels (over 90%) was found with the use of existing tabulations [46]. For the calculations shown, the percentage contributions to the broadening were approximately as follows: elastic collisions (17%), inelastic collisions (50%), strong collisions (33%). Theoretical reasons for the discrepancies between measurement and calculation could include any of the following: neglected contributions to the strong collision term (mainly monopole), the neglect of broadening by ion perturbers, and the complexity of such a many-electron atomic system as Kr III, which is treated only very crudely here, and for which optically forbidden collision-induced transitions (neglected here) may play a significantly more important role than assumed. On the latter point, the reader may wish to consult a discussion of a distorted-wave calculation by Hey and Blaha of the electron impact broadening of a prominent line in the N II spectrum [47].

For comparison of the calculated values with experimental Stark widths their ratios are given in Table I. The theoretical widths systematically underestimate the experimental

TABLE I. Experimental Stark widths (FWHM) of the Kr III ions for the $J=2-1$, $J=2-2$, and $J=2-3$ components originating from the multiplet ($5s\,^5S^o - 5p\,^5P$) and comparison with theoretical values of Hey and Breger [6]. The experimental values correspond to measurements in second and third order.

Density n_e (10^{18} cm^{-3})	Temperature $k_B T_e$ (eV)	Expt. Stark width w_{expt} (0.1 nm)	w_{expt}/w_{HB}
0.53 ± 0.10	3.20 ± 0.48	1.14 ± 0.17	1.76
0.65 ± 0.08	3.70 ± 0.55	1.15 ± 0.14	1.47
0.66 ± 0.17	3.67 ± 1.03	1.22 ± 0.17	1.53
0.71 ± 0.15	3.50 ± 0.68	1.14 ± 0.13	1.32
1.02 ± 0.10	4.30 ± 0.45	1.41 ± 0.10	1.16
1.16 ± 0.12	4.90 ± 1.56	1.81 ± 0.18	1.33
1.39 ± 0.15	5.30 ± 0.67	1.76 ± 0.09	1.09

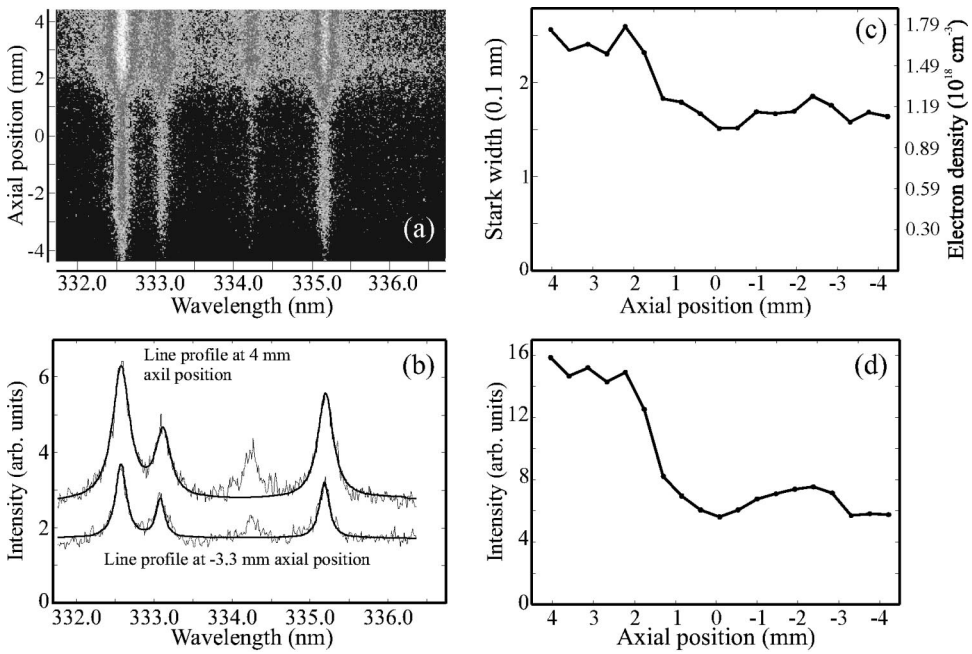

FIG. 4. (a) An example of an ICCD spectrum with inhomogeneous emission along the z axis recorded in second order. (b) Averaged profiles at the axial positions as stated in the figure. The Stark width, FWHM (c) and intensity (d) of the transition at $\lambda=332.575$ nm (J=2−2) vs axial position. The electron density stated at the right margin is determined from Eq. (2.2).

results, which might be attributed to the mentioned deficiencies, especially the missing of energy levels higher than 6s. Nevertheless, the agreement is good especially for the data points measured at higher densities.

B. Large amount of injection

The above scaling law was established from a homogeneous plasma column by injecting a low-to-moderate amount of test gas ($n_{\mathrm{imp}}<1\%$ of n_e). The homogeneity could be seen on the spatially resolved spectral lines; for examples see Figs. 2(a) (first order) and Fig. 2(c) (third order). In former measurements inhomogeneities along the z axis had been cultivated by injection of large amounts of test gas leading to population inversion [48]. In order to investigate effects of high test gas injection on the plasma homogeneity we injected an order of magnitude more test gas resulting in an impurity concentration of about 3% of the electron density. An example of an ICCD spectrum in second order with an inhomogeneous emission along the z axis is shown in Fig. 4(a). The line intensity is, in contrast to Figs. 2(a) and (2c), not homogeneously distributed along the z axis but forms two different plasma regions. In contrast to the homogeneous line emission shown in Fig. 2(a) and Fig. 2(c) we now increased the slit height of the spectrograph. For the homogeneous condition a small slit height is useful in order to suppress stray light in the spectrograph while the large slit size in the inhomogeneous case allows one to cover a larger volume to study the variation of the plasma parameters.

When investigating the spatial structure it is of utmost importance to focus a sharp image of the plasma column onto the entrance slit of the 1-m spectrograph. With a 1:1 magnification and taking into account the resolving limit of 3 pixel of the ICCD camera a spatial resolution of about 60 μm along the z axis is achieved. However, each single channel is too noisy to be fitted reliably with a theoretical profile. Therefore, we took the average of 20 vertical channels in order to improve the signal-to-noise ratio, which resulted in an average spatial resolution of 460 μm. In Fig. 4(b) the average spectra around the position -3.3 mm and 4.4 mm are plotted. For this discharge condition we found that in some spectra the line at the wavelength of $\lambda=335.193$ nm is affected by some unidentified lines and it was difficult to isolate the true Stark width of this line. The stronger component (332.575 nm, $J=2-2$) is not affected, however, it is not possible to state exact intensity ratios. In Figs. 4(c) and 4(d) the Stark width and intensity of the $J=2-2$ component are shown along the axis of the plasma column. We used the above derived scaling law [Eq. (2.2)] to determine the electron density from the Stark width. For the different axial positions, the corresponding density is also given in Fig. 4(c). Thomson scattering corresponding to the shown spectrum yields an electron density of 1.49×10^{18} cm^{-3}, which is not spatially resolved. This density is consistent with the axially resolved density determined from the Stark width.

It is typical for cases with injection of a large amount of test gas that the density varies by a factor of 1.6 over a distance of 2 mm. On the same scale the intensity in Fig. 4(d) varies by a factor of 3. In some spectra the latter grows even by a factor of 6 while the density variation approximately remains the same. Figures 4(c) and 4(d) reveal that the variation pattern of both intensity and width along the axis is similar, however, the intensity variation is stronger than that of the width. Without knowledge of the spatially resolved electron temperature, two explanations are most likely: first, the comparatively large reduction of the intensity may be the result of an increase or a decrease of the temperature in that region of the plasma column that leads to a reduction of Kr III ions compared to other Kr ionization stages. Second, due to a constriction there are simply fewer Kr ions and fewer plasma particles along the line of sight. Both explanations can be attributed to instabilities. Since the inhomogeneous emission of the spectral line is connected with the injection of a large amount of test gas, the variation of plasma conditions along the axis can be explained by a Rayleigh-Taylor instability. A large amount of injected test gas will more strongly decelerate the imploding plasma col-

umn, resulting in an enhanced growth rate of the instability [49]. In order to investigate this instability in detail axially resolved plasma parameters have to be known.

CONCLUSION

We have presented an experimental scaling law of the Stark width of three components of the $(5s\,^5S^o - 5p\,^5P)$ transition in Kr III. This scaling law can be used to determine the electron density in other applications. A comparison with theoretical Stark widths gives good agreement, bearing in mind the incompleteness of atomic energy levels of Kr III. A reasonably good linear dependence of the experimental Stark width on the electron density supports the absence of Doppler broadening of spectral lines and of hydrodynamic turbulence in the plasma. In a second experiment we have shown that inhomogeneities can be cultivated in the plasma by injecting a large amount of test gas. The resulting density variation along the axis is revealed by applying the above density/width relation. This variation can be attributed to an increased growth rate of the Rayleigh-Taylor instability, which appears when injecting large amounts of test gas.

ACKNOWLEDGMENTS

The work was supported by the Sonderforschungsbereich 191 of the DFG. The authors thank J. D. Hey for the calculations and discussions. One of us (I.A.) thanks the DAAD for support.

[1] K. Shimoda, in *Introduction to Laser Physics*, Springer Series in Optical Sciences Vol. 44 (Springer, Berlin, 1984).
[2] M. A. Cayless and A. M. Marsden, in *Lamps and Lighting*, 3rd. ed. (Publishers Edward Arnold, London, 1983).
[3] J. Davis, Nav. Res. Rev. A **3**, 36 (1989).
[4] P. H. Rebut (unpublished).
[5] U. Samm, Trans. Fus. Tech. **33**, 273 (1998).
[6] J. D. Hey (private communication).
[7] J. D. Hey and P. Breger, J. Quant. Spectrosc. Radiat. Transf. **24**, 349 (1980).
[8] J. D. Hey and P. Breger, J. Quant. Spectrosc. Radiat. Transf. **24**, 427 (1980).
[9] A. Trigueiros, S. G. Pettersson, and J. G. R. Almandos, Phys. Scr. **34**, 164 (1986).
[10] A. G. Trigueiros, C. J. B. Pagan, S. G. Pettersson, and J. G. R. Almandos, Phys. Rev. A **40**, 3911 (1989).
[11] B. C. Fawcett and G. E. Bromage, J. Phys. B **13**, 2711 (1980).
[12] A. E. Livingston, L. J. Curtis, R. M. Schectman, and H. G. Berry, Phys. Rev. A **21**, 771 (1980).
[13] J. G. R. Almandos, F. Bredice, M. Raineri, M. Gallardo, and A. Trigueiros, J. Phys. B **29**, 5643 (1996).
[14] M. Gallardo, F. Bredice, M. Raineri, J. R. Almandos, S. G. Petterson, and A. G. Trigueiros, Appl. Opt. **28**, 5088 (1989).
[15] J. Reader, N. Acquista, and V. Kaufman, J. Opt. Soc. Am. B **8**, 538 (1991).
[16] H. R. Griem, Y. V. Ralchenko, and I. Bray, Phys. Rev. E **56**, 7186 (1997).
[17] S. Glenzer, N. I. Uzelac, and H.-J. Kunze, Phys. Rev. A **45**, 8795 (1992).
[18] S. Glenzer, J. D. Hey, and H.-J. Kunze, J. Phys. B **27**, 413 (1994).
[19] F. Böttcher, J. Musielok, and H.-J. Kunze, Phys. Rev. A **36**, 2265 (1987).
[20] S. Glenzer, J. Musielok, and H.-J. Kunze, Phys. Rev. A **44**, 1266 (1991).
[21] S. Glenzer and H.-J. Kunze, Phys. Rev. E **49**, 1586 (1994).
[22] I. Olivares and H.-J. Kunze, Phys. Rev. E **47**, 2006 (1993).
[23] Th. Wrubel, S. Glenzer, S. Büscher, and H.-J. Kunze, Astron. Astrophys. **306**, 1023 (1996).
[24] J. Musielok, F. Böttcher, H. R. Griem, and H.-J. Kunze, Phys. Rev. A **36**, 5683 (1987).
[25] A. Gawron, S. Maurmann, F. Böttcher, A. Meckler, and H.-J. Kunze, Phys. Rev. A **38**, 4737 (1988).
[26] J. D. Hey, A. Gawron, P. Breger, and H.-J. Kunze, J. Phys. B **22**, 241 (1989).
[27] St. Böddeker, S. Günter, A. Könies, L. Hitzschke, and H.-J. Kunze, Phys. Rev. E **47**, 2785 (1993).
[28] S. Büscher, S. Glenzer, Th. Wrubel, and H.-J. Kunze, J. Quant. Spectrosc. Radiat. Transf. **54**, 73 (1995).
[29] S. Büscher, S. Glenzer, Th. Wrubel, and H.-J. Kunze, J. Phys. B **29**, 4107 (1996).
[30] H. R. Griem, *Principles of Plasma Spectroscopy* (Cambridge University Press, Cambridge, 1997).
[31] M. S. Dimitrijević and N. Konjević, J. Quant. Spectrosc. Radiat. Transf. **24**, 451 (1980).
[32] S. Alexiou, Phys. Rev. Lett. **75**, 3406 (1995).
[33] S. Glenzer, in *Atomic Processes in Plasmas*, edited by A. L. Osterheld and W. H. Goldstein, AIP Conf. Proc. No. 381 (American Institute of Physics, New York, 1996), Vol. 10, p. 109.
[34] S. Glenzer and H.-J. Kunze, Phys. Rev. A **53**, 2225 (1996).
[35] K. H. Finken and U. Ackermann, Phys. Lett. **85A**, 278 (1982).
[36] K. H. Finken and U. Ackermann, J. Phys. D **15**, 615 (1982).
[37] K. H. Finken and U. Ackermann, J. Phys. D **16**, 773 (1983).
[38] H.-J. Kunze, in *Proceedings of the 8th International Conference on Spectral Lineshapes, Williamsburg, Virginia, 1986*, edited by R. J. Exton (A. Deepak Publishing, Hampton, 1987), Vol. 4.
[39] Th. Wrubel, S. Büscher, I. Ahmad, and H.-J. Kunze, in *Proceedings of 11th APS Topical Conference on Atomic Processes in Plasmas, Auburn* (AIP Press, Woodbury, NY, 1998).
[40] Th. Wrubel, I. Ahmad, S. Büscher, and H.-J. Kunze, *Proceedings of the 4th International Conference on Dense Z-Pinches, May 28–30, 1997*, Vancouver, CP409, edited by N. R. Pereira, J. Davis, and P. E. Pulsifer (AIP Press, Woodbury, NY, 1997), p. 455.
[41] H. R. Griem, *Plasma Spectroscopy* (McGraw-Hill, New York, 1964).
[42] W. L. Wiese, M. W. Smith, and B. M. Glennon, *Atomic Transition Probabilities* (National Bureau of Standards and Technology, Washington, DC, 1966).
[43] A. R. Striganov and N. S. Sventitskii, *Tables of Spectral Lines of Neutral and Ionized Atoms* (IFI/Plenum, New York, 1968).

[44] Schott Optische Glasfilter Manual, Schott Glaswerke, Mainz, Germany.
[45] H. Van Regemorter, Astrophys. J. **136**, 906 (1962).
[46] J. Sugar and A. Musgrove, J. Phys. Chem. Ref. Data **20**, 859 (1991).
[47] J. D. Hey and M. Blaha, J. Quant. Spectrosc. Radiat. Transfer **20**, 557 (1978).
[48] S. H. Glenzer, Th. Wrubel, H.-J. Kunze, and L. Godbert-Mouret, Phys. Rev. E **55**, 939 (1997).
[49] J. S. De Groot and A. Toor, Phys. Plasmas **4**, 737 (1997).